# *Numerical investigation of effects of PFCDs geometry on the flow field and heat transfer of air flow in solar chimney power plant*

1st Kebabsa.H, 2nd Lounici.MS

*LEMI, Université M'Hamed Bougara,*

*Boumerdes, 35000 Algeria.*

KEBABSA_HAKIM@YAHOO.COM

***Abstract*—In this paper, the effects of PFCDs geometry on the flow field and heat transfer are studied when they are used in the solar chimney. For this purpose, the $SST/k-\omega$ model, has been employed. The simulation results have indicated that the $SST/k-\omega$ model has a close agreement with the available experimental data. Results are performed in terms of mean velocities and global parameters, i.e., strain rate, Reynolds shear stress. Results from numerical simulations, using different configurations, show that the flow field and the corresponding heat transfer distribution are affected by PFCDs geometry. Also, PFCDs position affects the flow structure and consequently the heat transfer. Heat transfer rate experiences several extreme as a result of fluid mixing emergence, agitation and flow pattern guidance of PFCDs.**

***Keywords*—*Passive flow control, CFD, Solar chimney power plants, Numerical simulation.***

## I. INTRODUCTION

Extensive fossil fuel exploitation led to global warming, the greenhouse effect, climate change, ozone layer depletion, and acid rain. Replacing fossil fuel usage as much as possible with environmentally friendly, clean, and renewable energy sources is a key to avoid further impacts of these phenomena. Among these sources, solar energy is the more abundant than other types of renewable energy such as wind, geothermal, hydropower and biomass. The solar chimney power plant system (SCPPS) has been investigated all over the world since the German researcher Jorg Schlaich made the brainchild in the 1970s. The SCPPS, due to its attractive advantages of being lower maintenance expense, clean, and longer operational life span, has excited many researchers all over the world, especially in countries with arid areas. The system is composed of: chimney, collector and turbine. A schematic of the SCPP is shown in Fig.1.

Schlaich developed the first concept and put the prototype in operation during the 1980s [1,2], Since then, various SCPP prototypes have been built in order to analyze its performance [3,4]. Due to the good characteristics of the technology, experiments of the SUPPS have greatly promoted practical applications for the technology. In this context, several researches have been presented to design and optimize the solar setup [5]. Maia et al. [6] built and tested a solar chimney in Brazil, with a tower height of 12.3 m and a collector diameter of 25 m. Zhou et al. [7] reported a pilot experimental solar chimney power setup in Wuhan, China. Results showed that the temperature difference between their collector outlet and the ambient air was 24.1 °C. Kasaeian et al. [8] presented a solar chimney pilot power plant with a 10 m collector diameter and 12 m chimney height. Results showed that a steady air flow was created by increasing the day temperature. The same phenomenon was also verified by Ghalamchi et al. [9,10]. Kalash et al. [11] examined the performance of a small-size sloped SUPPS in Syria. Bugutekin [12] analyzed the effect of environmental temperature, the chimney height and solar radiation on the performance of SCPP.

In 2011, Najmi et al. [13] built a small-scale solar chimney in Kerman, Iran. The authors studied effective parameters to optimize the solar chimney performance. They concluded that a decreased collector height to 1.3 m, and divergent tower increase the power output. In 2015, Kasaeian et al. [14] investigated a small solar chimney with 2 m height and 3 m collector diameter. Results showed that reduced entrance size enhance the system performance. In 2015, Okada et al. [15] used a divergent tower to increase the velocity of the air in the turbine. It was found that this model increased the power output by 2.6– 3.0 times higher than the convectional type.

Many mathematical models to assess the overall performance of SUPPSs have been reported in the last few decades. Bernardes et al. [16] developed a mathematical model to describe the thermal behaviour and output power performance of a large scale SUPPS. Ming et al. [17] conducted further research into the influence of various geometric parameters on the driving force and the power output of SUPPSs.

With the rapid development of computational prediction, research publications using CFD methods on SUPPSs occupy the mainstream in this field. Ming et al. [18] numerically analyzed the SUPPS's performance. Koonsrisuk et al. [19] investigated the changes in flow characteristics caused by geometric parameters variations using CFD. They found that tilting collector performed better than a conventional system. Kasaeian et al. [20] numerically analyzed the effects of geometrical parameters on a constructed solar chimney power plant. Fasel et al. [21] simulated the fluid dynamics and heat transfer mechanisms in SUPPSs using ANSYS. Results indicated that the flow in the chimney was fully turbulent. Al-Kayiem et al. [22] presented a mathematical model and analyzed the thermal energy and fluid flow within a SUPPS with an inclined roof, which was further validated by experiments. Recently, CFD analysis can be found in the following research articles [23,24].

In the recent years, Flow control is a major field of fluid mechanics [25]. It is very promising in the manipulation of fluid flow behaviour. This involves a slight configuration change for an important engineering benefit. Flow control can be a critical enabler to improve efficiency and performance and to save energy like mixing enhancement, lift increase, improvement of industrial processes in which fluid flows or heat transfer convection are present. The solar chimney power plant which based on heat transfer convection is a system where passive flow control could make an appreciable difference.

The present work investigates the influence of passive flow control devices on the flow field. Geometric parameters such as, collector inlet height, tower radius ratio were tested to improve the performance of SCPP.

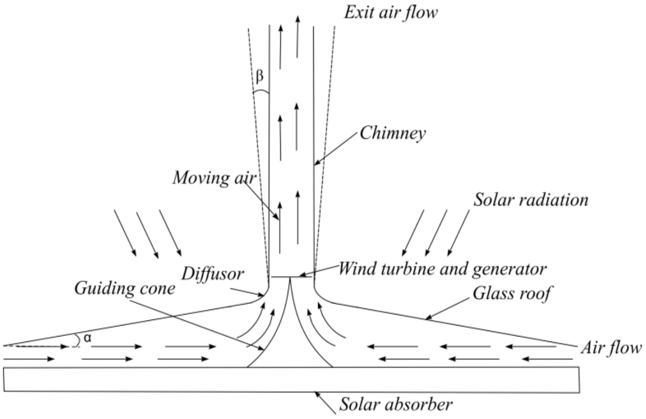


**Fig. 1.** *Solar chimney power plant system.*

## II. Methodology

### A. Case study description

**Geometric configuration.** The schematic diagram of the geometry and solution domain is shown in Figure 2.

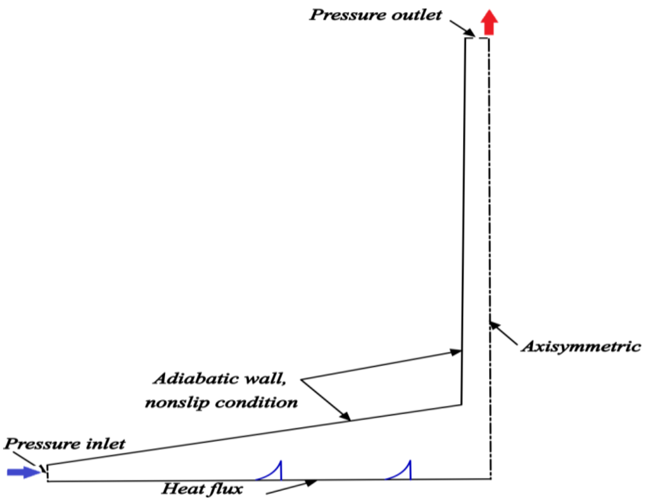


**Fig. 2.** *Schematic diagram of the geometry and solution domain.*

The experimental setup of references [26and27] is selected for the validation of the present simulations. The axially symmetric solution domain was modeled with a 2-D axisymmetric calculation based on the axisymmetric assumption of the configuration investigated, as shown in Fig 2.

The experimental data considered for the numerical model validation represent one working hour on 7th September, (i.e. 11:00). The physical properties of air have been considered in the temperature of 23°C. Figure 2 illustrates a schematic of the computational geometry and boundary conditions used in the present study.

A 2D model was created with the quadrilateral (structured) grid to study thermo hydrodynamic characteristics of the airflow as shown in Figure 2. The turbine is not considered in this study.

**TABLE I.** GEOMETRY OF SCPP

| Description | Dimension (m) |
|---|---|
| Inlet height | 0.05 |
| Outlet height | 0.5 |
| Collector radius | 12.5 |
| Tower entrance height | 1.5 |
| Tower height | 10.8 |
| Chimney radius | 0.5 |

The dimensions of the physical domain are shown in Table 1.

### B. *Mathematical formulation*

ANSYS FLUENT 16.0, commercial (CFD) software, was used for simulation purpose in this study.

Different turbulence models have been developed to predict natural convection flow properties. In this work, the shear stress transport k-ω model is employed. The SST model combines the original Wilcox k-w model for use near walls and the standard k–ε model away from walls.

The basic governing equations to be solved are the RANS equations, including the mass, momentum, and energy conservation equations.

The standard Boussinesq hypothesis is used to relate the Reynolds stresses to the mean velocity gradients.

The integral form of governing equations for a steady, incompressible and turbulent flow with constant properties is defined as:

$$\frac{\partial \rho}{\partial t} + \nabla \cdot \left(\rho \vec{v}\right) = S_m$$

$$\frac{\partial}{\partial t}\left(\rho \vec{v}\right) + \nabla \cdot \left(\rho \vec{v}\vec{v}\right) = -\nabla p + \nabla \cdot \left(\bar{\bar{\tau}}\right) + \rho \vec{g} + \vec{F}$$

$$\frac{\partial}{\partial t}\left(\rho H\right) + \nabla \cdot \left(\vec{v}\left(\rho H + p\right)\right) = \nabla \cdot \left(k_{eff} \nabla T\right) + S$$

$$\bar{\bar{\tau}} = \mu\left[\left(\nabla \vec{v} + \nabla \vec{v}^{T}\right) - \left(\frac{2\nabla}{3}\right) \cdot \vec{v} I\right]$$

In this formulation, the following have been assumed: incompressible Newtonian fluid, constant specific heat, nonparticipant radiant medium, and negligible effect of both body forces and viscous dissipation.

**Turbulence modeling.** The numerical model considered is based on the resolution of the Navier-Stokes equations in conjunction with the sst k-w turbulence model. These equations were solved by a finite volume discretization method. The Shear Stress Transport k–ω (SSTKW) model (Menter) contains a modified turbulent viscosity formulation to account for the transport effects of the principal turbulent shear stress. In the $SST/k-\omega$ model of Menter, a cross-diffusion term in the $\omega$ equation is implemented which influences $\omega$ to diffuse from the turbulent region to a non-turbulent region. Also, the $SST/k-\omega$ model has a blending function which causes the turbulence model behaves similar to the standard $k-\omega$ model in the near wall regions, while for areas away from the walls, switches to the $k-\varepsilon$ model.

The pressure-based solver was used to solve the equations with viscous dissipation and gravitation considered. The low- Re correction was activated to make a better simulation of the process of laminar-turbulent transition. The coupled scheme was used for the pressure–velocity coupling. The second order upwind scheme was used for the spatial discretization for all the variables. The calculation was regarded as converged when the scaled residual of the continuity, momentum, energy equations, $k$ equation and $\omega$ equation dropped by 5-7 orders of magnitude with very small changes with more iterations.

The boundary conditions for the computational domain are summarized in Table 2.

**TABLE II.** THE BOUNDARY CONDITIONS FOR NUMERICAL SIMULATIONSs.

| Place | Type | Description |
|---|---|---|
| Centerline | Axis | Symmetry |
| Ground | Wall | Q |
| Collector | Wall | Q = 0 |
| Tour | Wall | Q = 0 |
| Inlet | Pressure inlet | $P_{atm}$ |
| Outlet | Pressure outlet | $P_{atm}$ |

***Grid Generation.*** In order to prove the simulation results are independent of mesh size, three mesh sizes of (26x356), (52x712) and (78x1068) were used. Structured grids were made. The advantages that quadrilateral meshes have shown over the tetrahedral meshes are the lower overall cell count, almost five times lower than the original one, and a faster convergence. The coarsest grid #1 consisting of (26x356) quadrilateral cells was the base for progressive refining. Grid independence was evaluated on the basis of mass flux rate at the outlet of the system. Grid #2 (52x712) was found to provide sufficient resolution since the mass flux rate values at the selected boundary for grid #2 and #3 found to deviate by only 0.03%. The selected grid is concentrated near solid walls.

For each case, the near wall spacing was held constant, which resulted in $y+$ values no larger than 5.0. This was important due to that fact that enhanced wall functions were used in the turbulence model, which required the $y+$ values not to exceed 5 for results of the highest accuracy.

***Description of cases.*** Two configurations of incorporation of PFCDs are studied numerically in this paper. The first involve incorporation of these devices on the ground and the second under the collector.

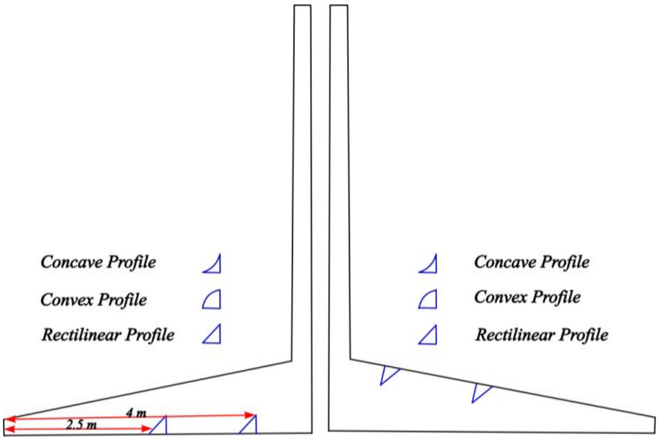


**Fig. 3.** *Shematic of PFCDs implementation.*

## III. Results and discussion

The numerical simulation results are presented in this section.

*A. Case study description Validation of base case.*

In this section, firstly a comparative study of temperature distribution is investigated and validated against the available experimental observation [26]. The numerical simulations were validated by simulating the air flow in the system as studied in the experiments of Nia et al. [27] with a 2-D axisymmetric model.

Figure 4 compares the temperature distribution along the collector, with the experiments and the numerical results of Nia et al. [27]. As shown in Figure 4, the tendency of temperature distribution, of the present simulations was consistent with the experiments of [27]. In the regions far away from the center of the system, the numerical simulations are in a good agreement with the experiment, the model has 0.1% deviation in predicting the temperature, while near the center of the system, the difference increases between these two; the numerical simulations and the experimental data as a result of developing turbulence and consequently, it influences the dynamics of the vortices. The maximum difference between the numerical results obtained and Nia experimental values was roughly 1.86%. It is observed that the present simulations have a suitable agreement with the available experimental data.

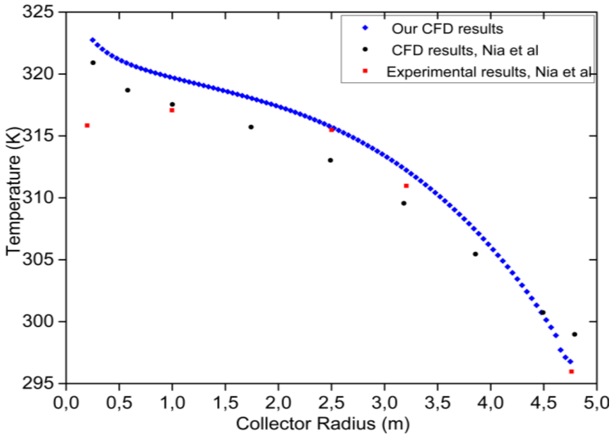


**Fig. 4.** *Temperature distribution along the collector, CFD against experimental data.*

This study considers 3 types (profiles) of PFCDs namely, concave, convex and rectilinear which implemented once on the ground and the other under the roof as shown in Figure 3. In all cases, each device was located at the same coordinate as presented in Figure3. The overall dimensions of devices must be selected in a manner to avoid obstruction of the flow development.

Different configurations are studied by means of Navier-Stokes simulations. In this technique, RANS model is explored with SST k-w platform. The main object of this work is to study numerical performance and accuracy of PFCDs implementation when they are used in the solar chimney. With this purpose, results from numerical simulations, using different configurations, are compared among them and with experimental data available in the literature. Comparisons are performed in terms of mean velocities and global parameters, i.e., the TKE. All simulations were performed using commercial software v16.0 FLUENT.

*B. Effects of PFCDs implementation on the ground*

Figure 5 shows velocity contours inside the system. It can be noted that the base case configuration produced the minimum velocity of all the cases. According to these results, it can be observed that the maximum velocity is recorded at the chimney base for the considered cases, where the observed static pressure drops significantly in accord with Bernoulli's principle due to eminent air flow and reaches a minimum value as shown in Figure 6. The maximum velocity magnitude varies from one configuration to another. In fact, it is noticed that the maximum velocity change shows a strong sensitivity to the change of devices profile as it does to the presence of PFCDs or not; it appears that the maximum difference is observed for the concave profile compared with the base case configuration. Indeed, it has been noted that the shape of PFCDs has a direct impact on the magnitude velocity of the air flow inside the SCPP. This favorable flow presented by velocity values can be explained in the following way. Different profiles of PFCDs produce different types of flow patterns in the system; PFCDs involve bringing more quantities of hot air to move upward and more quantities of cold air to go down. As the molecules are completely free to move, an important mixing process takes place. The dispersed fluid molecules allow a better exploitation of the energy inside the system and the mixing process reaches its maximum.

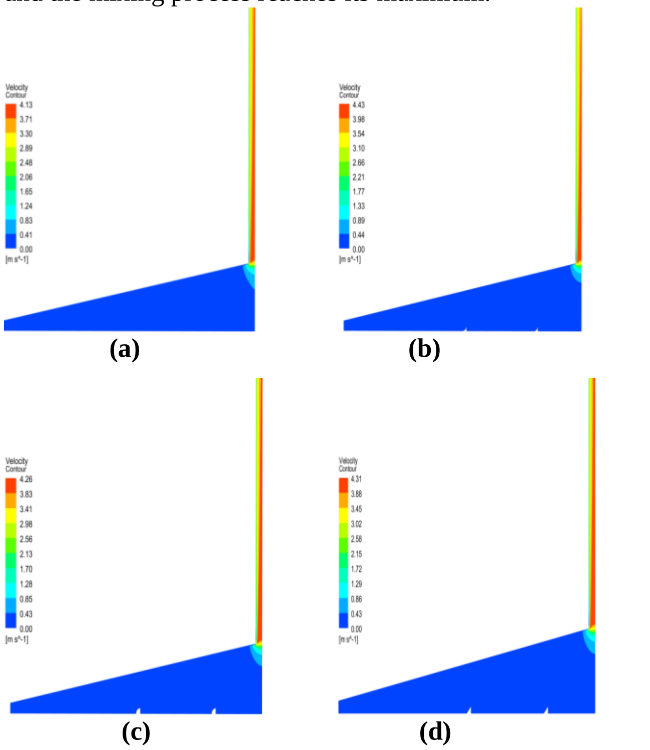


**Fig. 5.** *Mean velocity contour for (a) Base case (b) Concave (c) Convex (d) Rectilinear.*

By getting away from the inlet of the tour, all cases almost show similar trend. The three cases with concave, convex and rectilinear PFCDs show better velocity values than the base case as mentioned before. However, the highest velocity value is recorded when the concave profile is utilized. Geometric design of PFCDs improves flow field and heat transfer rate performance. In fact, the velocity improves about 7.5% on the total when concave profile is utilized.

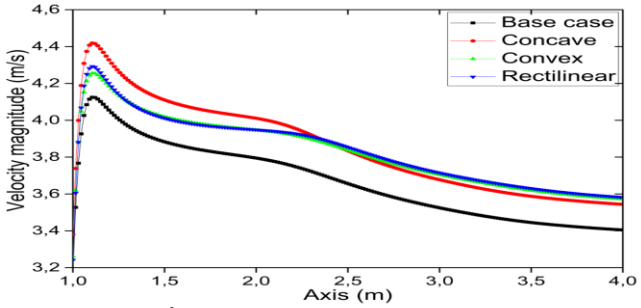


**Fig. 6.** *Plots of velocity magnitude throughout the chimney.*

The result showed that PFCDs characteristics influence the value of velocity especially when these devices were located on the ground. This finding suggests that the PFCDs profile has a significant role in energy transfer and as a result higher velocity magnitude is developed compared to base case. Considering the visual differences between the three cases profiles, it is not surprising that the mean flow characteristics predicted by utilizing these devices also differ significantly. The difference is clearly seen in Figure 6, which compares velocity magnitude distributions.

In this section, profiles of turbulent quantities are plotted to quantify some of the observations made earlier.

Figure 7 shows eddy viscosity contours for all cases. The recirculation which observed at the chimney entrance for the base case was enlarged. The large primary eddy in the base case would give rise to large velocity fluctuations but would have a low frequency. Such eddy account for the bulk of the kinetic energy present in the system.

Small eddy was formed behind the devices after flow passing the devices. Interaction between the primary eddy and slow moving streams created by the presence of PFCDs produces smaller eddies, which undergo further disintegration until, finally, dissipate their energy as heat as shown in Figure 7. Our premise is that comparisons of eddy viscosity from each case with the base case will give helpful local indications for improvement of the PFCDs.

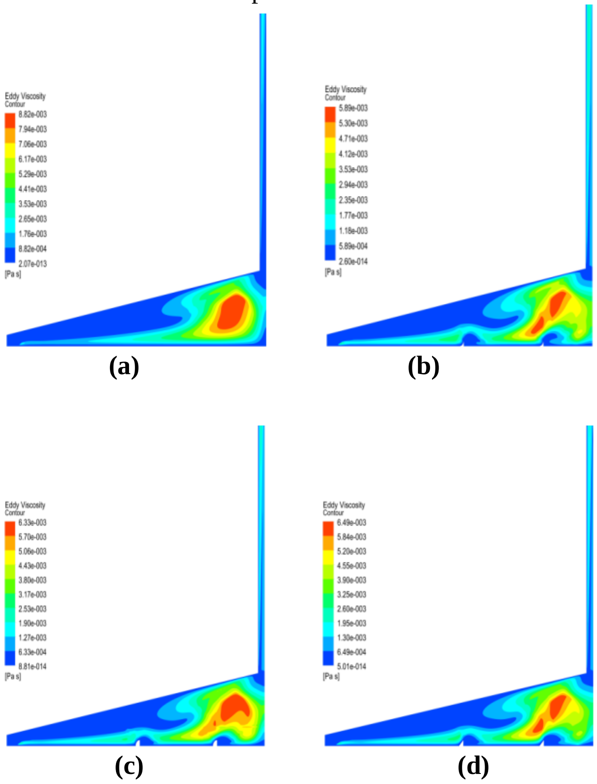


**Fig. 7.** *Eddy viscosity contours for (a) Base case (b) Concave (c) Convex (d) Rectilinear.*

A deeper insight into the effects of varying PFCDs profiles on flow is provided in Fig. 7. The presence of PFCDs creates instability that generates shear-layer vortices. These vortices decrease in size, and eventually dissipate in the chimney base. This latter observation indicates that there is better transport of air toward the chimney when using PFCDs.

For all cases, a local TKE maximum occurs in the region above the PFCDs location. For concave, convex and rectilinear cases, the peak (which differs in magnitude from one case to another) is directly above the PFCDs location. For concave, convex and rectilinear cases, dv/dx is large enough to produce negative –u'v'. Regarding the rate-of-dissipation, we note the tendency for it to mitigate the production since the rate of TKE production represents the work done against the mean-rate-of-strain field by the turbulent stresses.

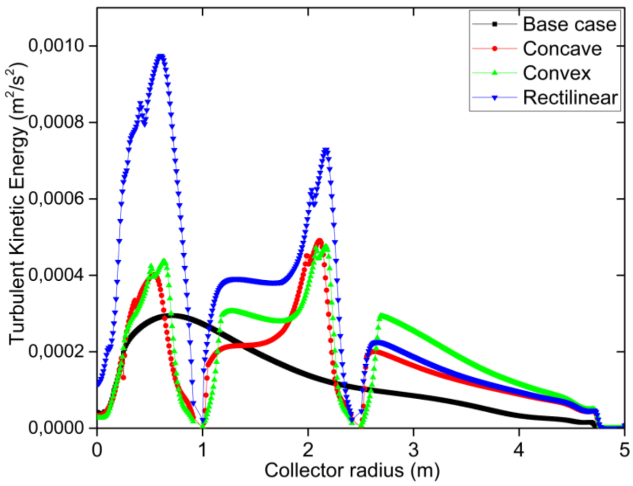


**Fig. 8.** *Turbulent kinetic energy ground for (a) Base case (b) Concave (c) Convex (d) Rectilinear.*

*C. Effects of PFCDs implementation under the collector*

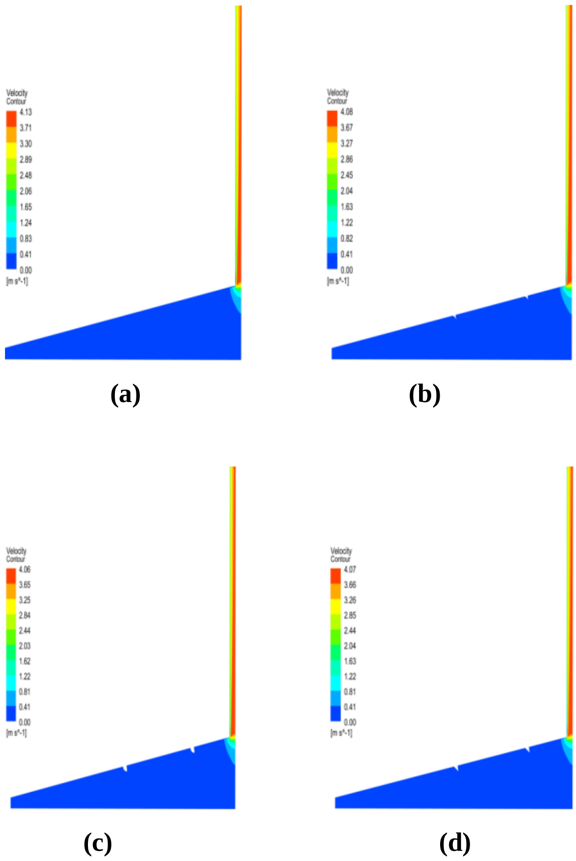


**Fig. 9.** *Mean velocity contour for (a) Base case (b) Concave (c) Convex (d) Rectilinear.*

When PFCDs are implemented under the collector, the velocity values are weaker than that of base case as shown in figure 9. Regions near the heated surface in the first configuration experience higher heat transfer rate in comparison to the second configuration; the higher heat transfer rate occurs in the bottom of the system as air flow pass by these devices. The above results confirm that the best performance of the heat transfer under the constant parameters takes place at the bottom (heated surface).

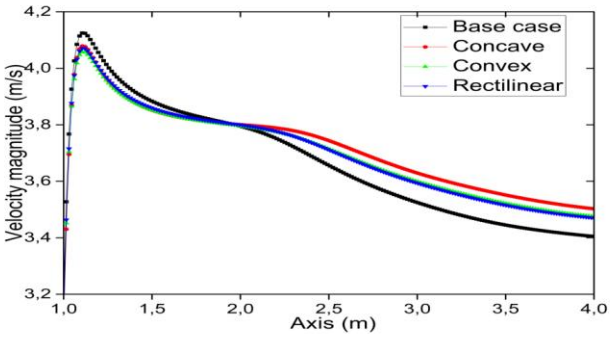


**Fig. 10.** *Plots of velocity magnitude throughout the chimney.*

The installation of these devices under the collector did not benefit the mean-flow characteristics as shown in figure 10; its result is in fact worse than that of the other one.

Eddy viscosity refers to the internal friction generated as laminar (smooth, steady) flow becomes irregular and turbulent as it passes over irregularities on the surface.

Figure 11 shows the eddy-viscosity contours. The figure illustrates a concrete mechanism responsible for the observed flow behavior.

It could be a kind of stability of the vortices, possibly related to vorticity "created" by the gradient of eddy viscosity, that results in the formation of bigger eddies.

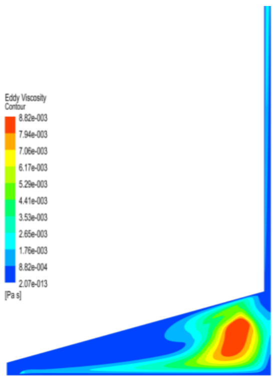

**(a)**

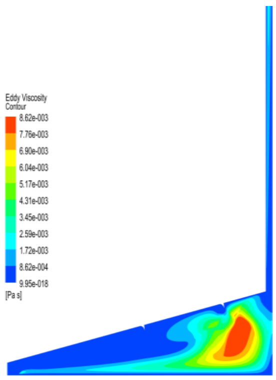

**(b)**

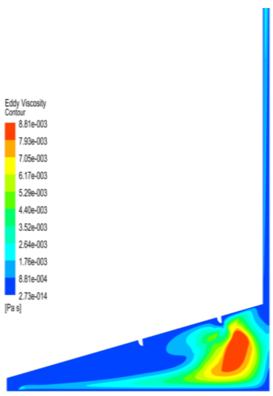

**(c)**

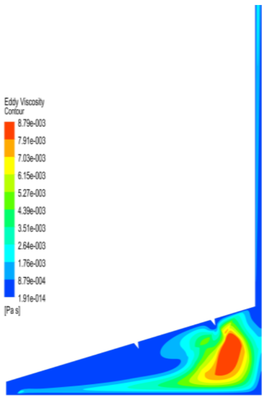

**(d)**

**Fig. 11.** *Eddy viscosity contours for (a) Base case (b) Concave (c) Convex (d) Rectilinear.*

For all cases, a local TKE maximum occurs in the region under the PFCDs location. For base, convex and rectilinear cases, the same tendency could be seen.

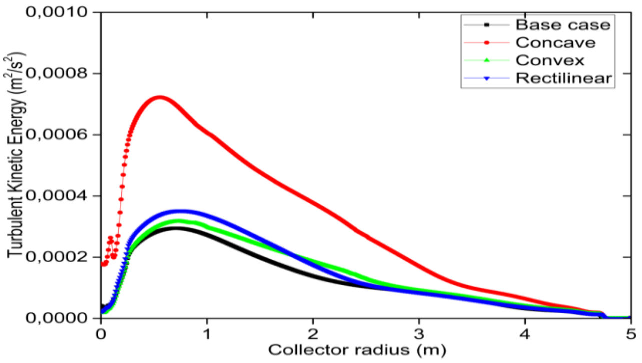


**Fig. 12.** *Turbulent kinetic energy for (a) Base case (b) Concave (c) Convex (d) Rectilinear.*

## CONCLUSION

In this paper, numerical simulations have been carried out to evaluate the influence of incorporation of passive flow control devices in solar chimney power plants.
From this study, we can draw the following conclusions:
-Implementation of the PFCDs under the collector reduces the thermal performances of the solar chimneys.
-Geometric design of PFCDs improves flow field and heat transfer rate performance. In fact, the velocity improves about 7.5% on the total when concave profile is utilized.
-PFCDs implementation on the ground is more beneficial.

## REFERENCES


[1] Schlaich J. The solar chimney. Edition Axel Menges. Stuttgart, Germany, 1995.

[2] Haaf W, Friedrich K, Mayr G, Schlaich J. Solar chimneys: part I: principle and construction of the pilot plant in Manzanares. Int J Sol Energy 1983;2: 3–20.

[3] Ferreira AG, Maia C.B, Cortez M.F.B, Valle R.M. Technical feasibility assessment of a solar chimney for food drying. Sol Energy 2008; 82:198–205.

[4] Maia C, Ferreira A, Valle R, Cortez M. Analysis of the Airflow in a Prototype of a Solar Chimney Dryer. Heat Transf Eng 2009; 30:393–9.

[5] Maia C, Ferreira A.G, Valle R.M, Cortez M.F.B. Theoretical evaluation of the influence of geometric parameters and materials on the behavior of the airflow in a solar chimney. Comput Fluids 2009; 38: 625–36.

[6] Maia C, Silva J.O.C, Cabezas-Gomez L, Hanriot S.M, Ferreira A.G Energy and exergy analysis of the airflow inside a solar chimney. Renew Sustain Energy Rev 2013; 27:350–61.

[7] Zhou X.P, Yang J.K, Xiao B, Hou G.X. Experimental study of temperature field in a solar chimney power setup. Appl Therm Eng 2007; 27: 2044–50.

[8] Kasaeian A.B, Heidari E, Vatan S.N. Experimental investigation of climatic effects on the efficiency of a solar chimney pilot power plant. Renew Sustain Energy Rev 2011; 15: 5202–6.

[9] Ghalamchi M, Kasaeian A, Ghalamchi M. Experimental study of geometrical and climate effects on the performance of a small solar chimney. Renew Sustain Energy Rev 2015; 2: 425–31.

[10] Ghalamchi M, Kasaeian A, Ghalamchi M, Mirzahosseini AH. An experimental study on the thermal performance of a solar chimney with different dimensional parameters. Renew Energy 2016; 91: 477–83.

[11] Kalash S, Naimeh W, Ajib S. Experimental investigation of the solar collector temperature field of a sloped solar updraft power plant prototype. Sol Energy 2013; 98: 70–7.

[12] Bugutekin A. An Experimental investigation of the effect of periphery height and ground temperature changes on the solar chimney System. Isi Bilim Ve Tek Derg-J Therm Sci Technol 2012; 32: 51–8.

[13] Najmi M, Nazari A, Mansouri H, Zahedi G. Feasibility study on optimization of a typical solar chimney power plant. Heat Mass Transf 2011; 48: 475–85.

[14] Ghalamchi M, Kasaeian A, Ghalamchi M. Experimental study of geometrical and climate effects on the performance of a small solar chimney. Renew Sustain Energy Rev 2015; 43: 425–31,

[15] Okada S, Uchida T, Karasudani T, Ohya Y. Improvement in solar chimney power generation by using a diffuser tower. J Sol Energy Eng 2015; 137: (3):031009.

[16] Bernardes M.A.D, Voss A, Weinrebe G. Thermal and technical analyses of solar chimneys. Sol Energy 2003; 75: 511–24,

[17] Ming T.Z, Liu W, Xu G.L. Analytical and numerical investigation of the solar chimney power plant systems. Int J Energy Res 2006; 30: 861–73.

[18] Ming T.Z, Wang X.J, de Richter R.K, Liu W, Wu T.H, Pan Y. Numerical analysis on the influence of ambient crosswind on the performance of solar updraft power plant system. Renew Sustain Energy Rev 2012; 16: 16:5567–83.

[19] Koonsrisuk A, Chitsomboon T. Mathematical modeling of solar chimney power plants. Energy 2013; 51: 314–22.

[20] Kasaeian A, Ghalamchi M, Ghalamchi M. Simulation and optimization of geometric parameters of a solar chimney in Tehran. Energy Convers Manag 2014; 83: 28–34.

[21] Fasel H.F, Meng L, Shams E, Gross A. CFD analysis for solar chimney power plants. Sol Energy 2013; 2: 12–22.

[22] Al-Kayiem H.H, Sreejaya K.V, Gilani S.I.U.H. Mathematical analysis of the influence of the chimney height and collector area on the performance of a roof top solar chimney. Energy Build 2014; 68:305–11.

[23] Guo P, Li J, Wang Y, Wang Y. Numerical study on the performance of a solar chimney power plant. Energy Convers Manag 2015; 105: 197–205.

[24] Guo P-h, Li J-y,Wang Y. Numerical simulations of solar chimney power plant with radiation model. Renew Energy 2014; 2: 24–30.

[25] Yagiz B. O, Kandil Y, Pehlivanoglu. Drag minimization using active and passive flow control techniques. Aerosp Sci Technol 2012; 17: 21–31.

[26] Kasaeian AB, Heidari E, Vatan SN. Experimental investigation of climatic effects on the efficiency of a solar chimney pilot power plant. Renew Sustain Energy Rev 2011; 15(9):5202–6.

[27] Nia Ehsan, Shabahang Ghazikhani M. Numerical investigation on heat transfer characteristics amelioration of a solar chimney power plant through passive flow control approach. Energy Conversion and Management 2015; 105:588–595.